Vis Geosci (2006) 11: 1–11
DOI 10.1007/s10069-006-0003-y

ORIGINAL ARTICLE

Dipesh Bhattarai · Bijaya B. Karki · Lars Stixrude

Space–time multiresolution atomistic visualization of MgO and $MgSiO_3$ liquid data

Received: 24 February 2006 / Accepted: 18 April 2006 / Published online: 27 June 2006

Abstract First-principles molecular dynamics simulations of complex material systems such as geophysically relevant oxide and silicate liquids produce massive amounts of time-varying three-dimensional data for the atomic configurations. Given the high accuracy of these data, it is desirable to extract as much information hidden in the data as possible. In this paper, we elaborate on our recently proposed scheme to support interactive visualization at space–time multiresolution of the atomistic simulation data. Instead of just focusing on direct rendering of the given data, additional data (containing more quantitative and qualitative information) that usually have to be extracted by some other means are extracted and rendered on the fly. This allows us to gain better insight into the global as well as local spatio-temporal behavior of the data in the context of bonding, radial distribution, atomic coordination, clustering, structural stability and distortion, and diffusion. We illustrate such visualization for the simulation data on the liquid phases of MgO and $MgSiO_3$—the two most abundant components of Earth's mantle. Our analysis shows that the structure and dynamics of both liquids change substantially with compression, with no discernible effects of temperature in most cases.

Keywords Scientific visualization · First principles molecular dynamics · Mantle minerals · Silicate liquids · Space–time dataset · Cluster analysis

D. Bhattarai · B. B. Karki (✉)
Department of Computer Science,
Department of Geology and Geophysics,
Louisiana State University, Baton Rouge, LA 70803, USA
E-mail: karki@csc.lsu.edu
Fax: +1-225-5781465

L. Stixrude
Department of Geological Sciences,
University of Michigan, Ann Arbor, MI 48109, USA

Introduction

In recent years, visualization has taken on an increased importance in better understanding of various types of data of substantial geophysical significance. One important class of data is related to computer modeling of Earth forming materials. Current trends in such computational studies demand visualization along three major directions: first, ever-larger sets of data are produced by large-scale simulations. The challenge is simply how to graphically render such massive datasets (Sharma et al. 2003). Second, a wide range of properties including structure, elasticity, rheology and melting of materials are now simulated on a routine basis. The challenge is how to fulfill different domain-specific requirements within single visualization framework (Humphrey et al. 1996; Kokaji 2003; Li 2005). Third, the simulation methods of common practice range from those based on empirical or simplified interatomic force models, to sophisticated quantum mechanical computations producing outputs with different levels of accuracy. In particular, the first principles molecular dynamics (FPMD) algorithm based on interatomic interactions derived within the quantum mechanical framework can typically deal with several tens to a few hundreds of atoms with relatively high accuracy (Chelikowsky et al. 2001; Trave et al. 2002; Alfe 2005; Stixrude and Karki 2005; Karki et al. 2006). The challenge is how to extract as much information as possible from such highly accurate datasets (Kokaji 1999, 2003).

One can find a huge amount of work related to atomistic (molecular) visualization for which numerous applications, both commercial and public domain, currently exist. The common examples include Molscript (Kraulis 1991), VMD (Humphrey et al. 1996), XcrysDen (Kokaji 1999, 2003), Atomsviewer (Sharma et al. 2003), CrystalMaker (http://www.crystalmaker.com) and amiraMol (http://www.amiravis.com/mol) commercial packages, and numerous other public domain systems such as Aviz, gOpenMol, VASP DataViewer,

PyMD, etc. Most systems exploit 3D graphics supported by desktop computers but some also support immersive and interactive visualization requiring specialized resources such as Immersadesk and CAVE. In general, the existing visualization systems share many features (e.g., Li 2005).

We have recently initiated the development of an effective–efficient scheme for the visualization of the atomistic simulation data at space–time multiresolution (Bhattarai and Karki 2006). The proposed scheme deals with the atomic positional data as a function of time. It is believed to represent a more complete visualization than what currently exist and to allow us to extract detailed quantitative and qualitative (structural and dynamical) information hidden in the data of high accuracy such as those produced by FPMD simulations. The aim of this paper is twofold: first is to present the essence of the proposed visualization scheme by working with important examples, and second is to report a detailed analysis of the structural and dynamic properties of the liquid phases of MgO and $MgSiO_3$—the most abundant phases of Earth's mantle, by visualizing recent FPMD simulation data (Stixrude and Karki 2005; Karki et al. 2006). To the best of our knowledge, no such systematic visual analysis has previously been reported, particularly, in the context of Earth's materials studies. It is also relevant to mention the fact that deep Earth materials are usually studied over a wide range of pressure and temperature conditions—characteristics of Earth's interior. As such, the high-pressure and high-temperature properties of these materials are governed by substantial structural and dynamical changes at atomic scale.

The paper is organized as follows: it first describes the nature of the simulation datasets used for visualization. The space–time multiresolution (STMR) atomistic visualization scheme is then presented. The simulated liquid data for MgO and $MgSiO_3$ are visualized in details. Finally, the paper contains conclusions.

Simulation data

In the past, first-principles simulations of Earth materials were mostly performed for crystalline systems in which the symmetry constrains the simulation size (often unit cells with periodic boundary conditions are used) as well as the atomic configuration (a few free positional parameters need to be considered explicitly). For example, MgO in its conventional simple cubic structure requires only eight atoms whose positions are fixed by the cubic symmetry. Now due to the rapid advances in the computational resources/capabilities, simulations of disordered systems such as liquids and defective crystals are increasingly becoming common and precise. Such simulations require much larger atomic systems and the crystal symmetry is violated partially or completely. For example, the data for the liquid MgO used in this study were obtained for a system of 216 atoms so that a discrete set of 648 (positional) degrees of freedom need to be explicitly taken into account. Unlike a perfect crystalline phase, the atomic positions of a liquid phase are strongly correlated but without any long-range order. Even the short-range (local) order is temporal to a great extent and transient fluctuations are expected to occur. As such, the liquid simulation can be treated according to the Ergodic hypothesis. Visualization of the highly correlated data at different resolutions of length and time allows us to gain insight into the complex structural and dynamical nature of the liquid state.

In FPMD, or more generally, in any molecular dynamics simulation, a system is initially defined by a group of properties that represent atomic positions, atomic types, and constraints that have to be satisfied (e.g., Allen and Tildesley 1987). Let A be the collection of $\{R, S, C\}$ describing the system. Here, $R = \{r_i \in X \subset \Re^3\}$ (X demarcates the simulation box) is the set of the atomic positions in the system, which can be considered as discrete degrees of freedom. $T = \{s \in \text{Types}\}$ is the set of the atomic types (for instance, Mg, Si and O atoms for silicate liquid). C is the set of constraints that has to be satisfied by the system. For example, the FPMD simulation based on canonical NVT ensemble, the number of atoms in the supercell (N), the volume (V), and the temperature (T) are fixed. As the simulation progresses, a new system configuration is generated. Collection of A's over a given simulation time duration describes the system dynamics, i.e., $D = \{A_t | 0 \leq t \leq \Im\}$. In essence, FPMD computes the trajectories, i.e., positions $\{r_i \mid i = 1, ..., N\}$ as a function of time t, of all the atoms by numerically integrating the Newton's equations of motion:

$$m_i \frac{\mathrm{d}^2 r_i}{\mathrm{d}t^2} = F_i,$$

where m_i is the mass of atom i and $F_i = \sum_{i \neq j} f_{ij}$ is the force on atom i due to all other atoms. In FPMD, these interatomic forces are derived from a fully self-consistent solution of the electronic structure problem within density functional theory (Hohenberg and Kohn 1964; Kohn and Sham 1965). Unlike the methods based on empirical or simplified potential models, such quantum mechanical method is computationally very intensive.

The simulation data considered here were generated for two geophysically important phases—liquid MgO and $MgSiO_3$ by a parallel FPMD program called VASP (Kresse and Furthmuller 1996), which was executed on Supermike Linux Cluster at Louisiana State University using 32–128 processors (http://www.cct.lsu.edu). The data are three-dimensional and time-dependent in the nature. They represent the snapshots of atomic configurations at different instants of time. For instance, liquid MgO data from simulation using a supercell of 216 atoms for 3 ps contain 3,000 time points each of which, in turn, contains 216 positional data. Two sets of MgO liquid data corresponding to two conditions of $V1 = 26.96$ Å^3,

$T1 = 3{,}000$ K (condition $V1T1$) and $V2 = 14.33$ Å^3, $T2 = 9{,}000$ K (condition $V2T2$) are visualized. The silicate data are for an 80-atom supercell and duration of 3 ps. Three sets of the silicate data corresponding to three conditions of $V1 = 64.60$ Å^3, $T1 = 3{,}000$ K (condition $V1T1$); $V2 = 45.22$ Å^3, $T2 = 4{,}000$ K (condition $V2T2$) and $V3 = 32.30$ Å^3, $T3 = 6{,}000$ K (condition $V3T3$) are visualized.

Atomistic visualization scheme

We approach the atomistic visualization problem along three lines: first is to analyze the spatial proximity of individual atoms to each other, and their collective tendency to form a structure. Given single atomic configuration dataset produced at some particular FPMD step, information about bonding, correlation, coordination and clustering is explored with generation and subsequent rendering of various types of additional data. Second is to analyze temporal proximity of atoms, which determines the dynamical behavior of the system. Atomic positions are rendered as a function of time and a variety of atomic displacement data are generated and visualized. Third is to integrate the two types of analyses to visualize how the proximity relationships among the atoms (spatial information) vary over time (temporal proximity). All spatio-characterization properties can be animated to have an instantaneous view of the dynamics. Moreover, the simulation data represent an ensemble so it is also preferable to visualize the time-averaged and finite-time-span behavior of the atomic structure and movement.

The proposed space–time multiresolution visualization model consists of several modules to support the three-types of analyses mentioned in previous paragraph (Fig. 1). These modules are broadly put into two categories, namely, complete data rendering and local/extracted data rendering. Implementation is done in a modular fashion using C, OpenGL and GLUT (Shreiner et al. 2004; http://www.opengl.org), and GLUI (http://www.cs.unc.edu/~rademach/glui). The input data representing a position–time series are first read into the memory and kept there throughout the visualization process. The additional data are generated on the fly and they are represented with specific data-structures (e.g., adjacency list representation for graphs) and dynamic memory allocation. It was shown that the interactive frame rates are achievable for the system sizes consisting of a few hundred atoms (Bhattarai and Karki 2006) in ordinary computing environment such as PC desktops.

Complete data rendering

Animation

Animation is used for a rapid navigation through the data to have a quick overview of the spatio-temporal behavior of the system. The atoms are rendered as spheres at their respective positions in 3D space at a given time. In this ball representation, the radius and color differentiate atomic types: green, blue and red spheres denote Mg, Si and O atoms, respectively. Animation is supported in ball-stick (with length-encoded bonds) and polyhedral (distortion-encoded polyhedra) representations and also with several other rendering modules, which are described later. All relevant properties are computed and rendered instantaneously for every time step so it's crucial to ensure that computations are done fast enough to maintain interactivity.

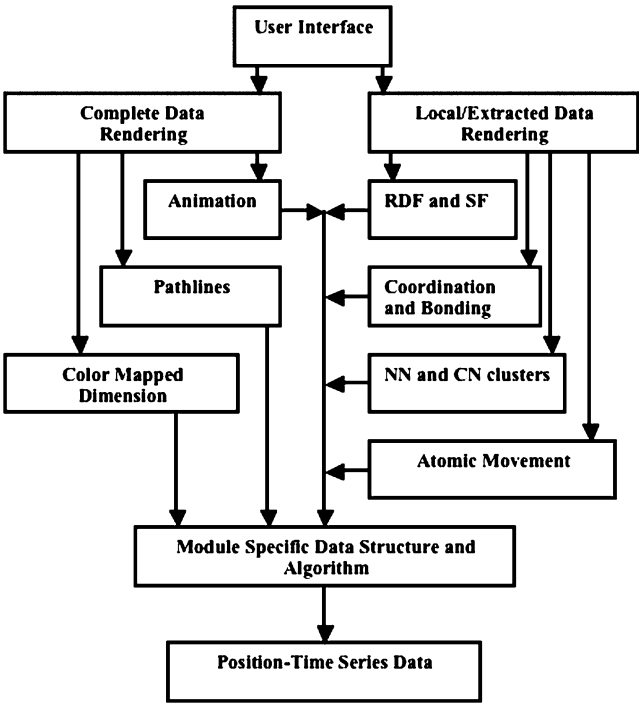

Fig. 1 Various visualization modules and their relationship among each other

Figure 2 shows snapshots of bonding and polyhedral structure in liquid oxide and silicate during the animation: bonds are shown between any two unlike atoms, whose separation falls between r_{START} and r_{MIN}, which are, respectively, the starting point and the minimum after the first peak of the Mg–O radial distribution function (see the subsection radial distribution function). Variation in the length (r) of a given bond is quantified using:

$$\lambda_B = \frac{(r - r_{START})}{(r_{MIN} - r_{START})}$$

which varies from 0 (when the atoms are separated by the minimum distance) to 1 (when the atoms are separated by the maximum distance). The cation coordination polyhedron such as SiO_n can be regarded as the fundamental structural unit. The degree of polyhedral distortion is characterized by using the following two parameters (Robinson et al. 1971; Thomas 1989):

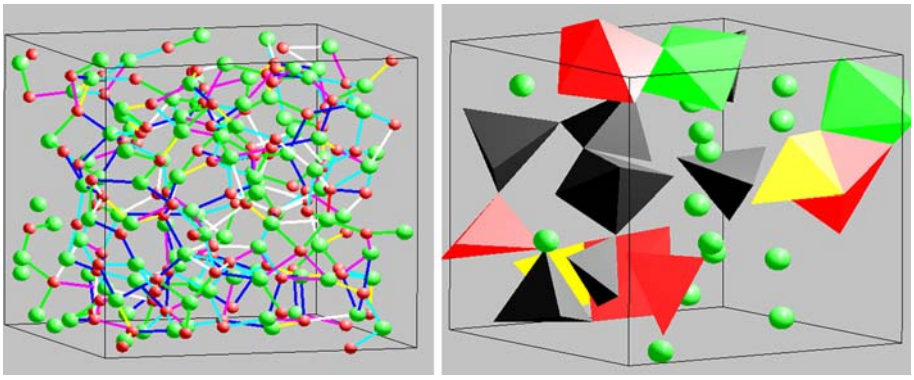

Fig. 2 Snapshot of the bond-length variation (λ_B) for oxide (*left*) and of quadratic elongation (λ_P) for silicate (*right*). Note that min = 0.0 and max = 1.0 for λ_B and min = 1.0 and max = 1.04 for λ_P

$$\text{quadratic elongation}, \lambda_P = \sum_{i=1}^{n} \frac{(l_i/l_0)^2}{n},$$

$$\text{bond-angle variance}, \sigma = \sum_{i=1}^{n} \frac{(\theta_i - \theta_0)^2}{n-1}.$$

Here l_0 and θ_0 are bond lengths and angles in a regular polyhedron, e.g., an octahedron, $n=6$ and $\theta_0=90°$. The bond length distribution and polyhedral distortion are visualized using the color-map scheme (Table 1) based on the corner values of the red–green–blue (RGB) color cube. For a given quantity (Q), we divide the range from its minimum (min) to maximum (max) values into eight equal intervals of size $d=(\text{max}-\text{min})/8$ so that we have the recursive relation given by $Q_i=Q_{i-1}+d$ with $Q_0=\text{min}$. In the case of bond-length, min = 0.0 and max = 1.0 so $d=0.125$. This color-map table is used to represent several other quantities derived later.

Pathlines

The complete trajectories of all or selected atoms are displayed as pathlines by connecting the successive positions for each atom by line segments. As an atom moves within the supercell satisfying the periodic boundary conditions, its path is traced using a color-coded line. The pixel color at a given position for a given atom is varied according to the elapsed time or the distance traveled by the atom relative to some reference position. Here, we track the movement of silicon and oxygen atoms of two SiO_n units in the silicate liquid during the simulation period of 2 ps (Fig. 3). Pathlines for oxygen atoms belonging to one polyhedron have entirely blue pathlines, indicating the stability of the corresponding Si–O bonds over the duration of the simulation. Another polyhedron from the same simulation shows substantial red portions of oxygen trajectories, showing that Si–O bonds of this polyhedron are broken, and the O atoms join other polyhedra. Also note that the Si atom of the tetrahedron has moved very little (yellow pathlines), compared to the Si atom of the octahedron.

Table 1 Eight colors with their red, green and blue components are used to represent eight values (intervals) of a given quantity. The case of bond-length variation is shown here

Color		(RGB)	Quantity (Q)	λ_B
Black		0 0 0	$min \le Q < Q_1$	0.000 – 0.125
Red		1 0 0	$Q_1 \le Q < Q_2$	0.125 – 0.250
Yellow		1 1 0	$Q_2 \le Q < Q_3$	0.250 – 0.375
Green		0 1 0	$Q_3 \le Q < Q_4$	0.375 – 0.500
Cyan		0 1 1	$Q_4 \le Q < Q_5$	0.500 – 0.625
Blue		0 0 1	$Q_5 \le Q < Q_6$	0.625 – 0.750
Magenta		1 0 1	$Q_6 \le Q < Q_7$	0.750 – 0.875
White		1 1 1	$Q_7 \le Q < max$	0.875 – 1.000

Color-mapped dimension

In the color-mapped dimension scheme, a four-dimensional space–time representation is reduced to a two-dimensional representation. A given atomic 3D position or displacement is mapped to a color value with red-component representing the x-coordinate, green-component representing the y-coordinate and blue-component representing the z-coordinate. The vertical and horizontal screen axes are used to represent the constituent atoms and simulation time, respectively. The pixel color at s_{ij}, which is the screen coordinate for ith atom at jth simulation step, is given by

$$C_{ij} = \text{color}\left[\mathrm{r_{ij}}, \mathrm{g_{ij}}, \mathrm{b_{ij}}\right],$$

where color components are given by

$$r_{ij} = \left(0.5 + f\left[x_{ij} - x_i^0\right]\right),\ g_{ij} = \left(0.5 + f\left[y_{ij} - y_i^0\right]\right)$$
$$\text{and } b_{ij} = \left(0.5 + f\left[z_{ij} - z_i^0\right]\right).$$

Here f is a scaling factor, x_{ij}, y_{ij}, z_{ij} define the 3D position of the ith atom at the jth timestep, and x_i^0, y_i^0, z_i^0 define the reference position of ith atom (such as crystalline or initial position or null). The individual pixels displayed on the screen thus represent individual 4D space–time data points. Unlike the direct 3D particle rendering, the reduced-2D representation does not suffer from any occlusion. Figure 4 shows the displacement of

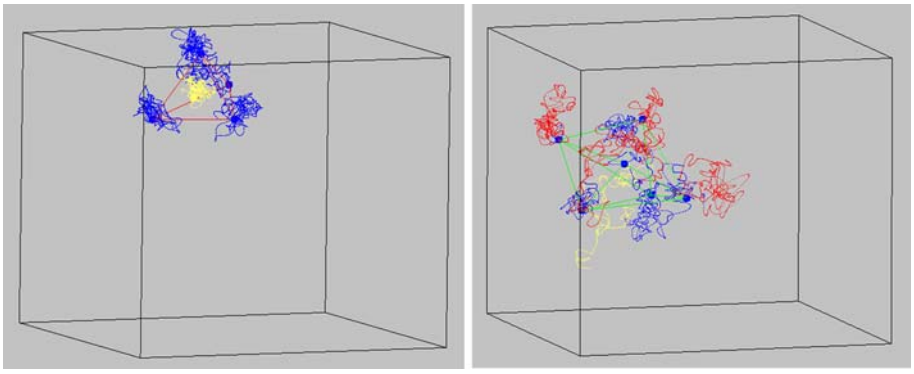

Fig. 3 Pathlines for two Si polyhedra. *Yellow lines* are for Si atoms. The *blue portion* of the pathline contains those positions of O atoms, which are within r_C from the Si atom whereas the *red portion* means the O atoms are at greater distances

atoms relative to the crystalline positions during the solid-to-liquid phase transition in a 64-atom MgO supercell.

Local/extracted data rendering

Radial distribution function

We compute the radial distribution function (RDF), $g(r)$, which determines the average density of atoms at a distance r from a specified atom. It thus represents an effective way of describing the average structure of disordered molecular systems such as liquids (Allen and Tildesley 1987). The RDF can be expressed as

$$g(r) = \frac{\rho^{2/N}(0, r)}{\rho^2},$$

where $\rho = N/V$ is the density of a system of volume V and N atoms, and $\rho^{2/N}$ $(0, r)$ is the probability that an atom is at r when there is another atom at the origin. The information such as the positions of the first peak (r_{PEAK}), the first minimum (r_{MIN}), and the distance averaged over the first peak in $g(r)$ out to the first minimum, r_{AVG} are used in various structural analysis modules. Also relevant is the window size of r_{BOND} defined as ($r_{\mathrm{MIN}} - r_{\mathrm{START}}$). The RDF of liquid MgO exhibits large fluctuations at small distances and approaches unity at larger distances indicating the short-range order and long-range disorder characteristic of the liquid state (Fig. 5). The structural factor (SF) is calculated by taking the Fourier transform of RDF.

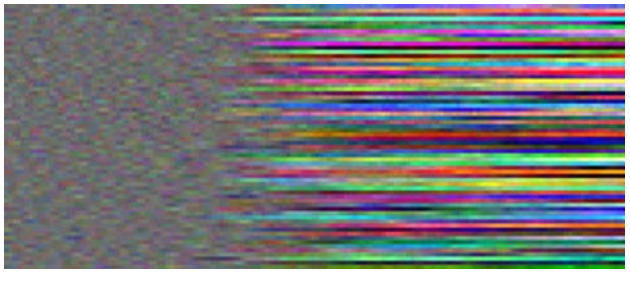

Fig. 4 Color-mapped dimension representation. *Gray region* on the left is the solid phase whereas the *brighter color region* on the right is the liquid phase. Atoms are grouped together vertically, with 32 Mg in the lower half and 32 O atoms in the upper half

Coordination environment

The simplest and most common parameter, which characterizes the local structural information, is the coordination number. The average coordination number, which indicates the average number of particles of species α around a particle of species β within a sphere of radius r_C, is simply an integral over the corresponding radial distribution function:

$$C_{\alpha\beta} = 4\pi\rho x_\beta \int_0^{r_C} r^2 g_{\alpha\beta}(r)\mathrm{d}r.$$

Here, ρ is the number density and x_β is the concentration (N_β/N) of atoms of type β. Since we are interested only in the nearest neighbors, the cutoff distance is often taken to be the first minimum (r_{MIN}) of the corresponding radial distribution function. FPMD simulations (Stixrude and Karki 2005; Karki et al. 2006) show that the average Mg–O and Si–O coordination

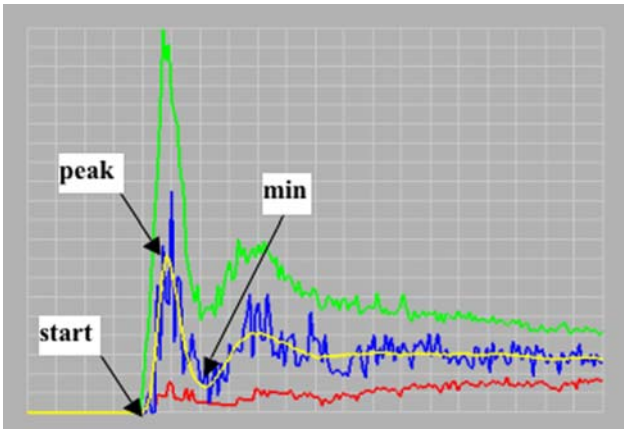

Fig. 5 Mg–O partial RDF (the *vertical axis*) for the liquid MgO as a function of distance, ***r*** (the *horizontal axis*). The *green* and *red* lines, respectively, show the maximum and minimum. The *blue line* is for a given time step. The *yellow line* is the averaged RDF for which the start, peak and minimum positions are indicated

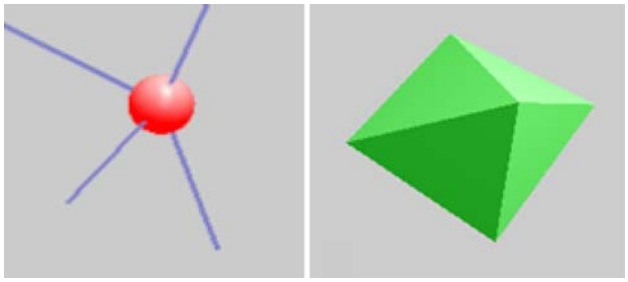

Fig. 6 Visualization of coordination using sphere (*red*: fourfold) and polyhedron (*green*: sixfold)

numbers increase smoothly and nearly linearly with compression, with no discernible influence of temperature. With increasing compression, C_{MgO} of liquid MgO increases from 5 at low pressure and exceeds 7 at pressures above 150 GPa. Similarly, C_{MgO} and C_{SiO} for the silicate liquid increase from 4 and 6, respectively, at low pressure to 6 and 8, respectively, at high pressure. We visualize the coordination environment as a function of space (per atom basis) in the form of simple sphere or polyhedral representation (Fig. 6) to gain insight into contribution of different types of coordination. The color-map (Table 1) is used to encode the local coordination number; black, red, yellow, green, cyan, blue, magenta and white represent coordination numbers ≤ 3, 4, 5, 6, 7, 8, 9, and ≥ 10, respectively.

Cluster analysis

Atomic clusters and their internal structures are extracted and rendered to obtain further insight into the local structure of a given system. If we can traverse through a group of atoms following a path from one atom to another atom such that the distance between any two consecutive atoms on the path are within a specified cutoff distance, then we say they are related in some fashion. For instance, one can extract a cluster (Fig. 7, left), which connects successive nearest neighbor atoms (Jarvis and Patrick 1973). Let $n_i = \{1 \leq j \leq n_a : d(i, j) \leq r_C\}$ be the set of the nearest neighbors of the atom i. Now, the NN cluster structure formed by the atom i can be defined as $i \cup k$, where k is recursively defined as $\{k \in n_i \vee k \in n_j \exists\ _j \in K\}$. Common-neighbor (CN) analysis is another important approach to understand the cluster internal structure (Blaisten-Barojas 1984; Honeycutt and Andersen 1987). It represents a way of decomposing the RDF according to the environment of the pairs. A pair is considered bonded if they are within the cutoff distance (r_C) of each other. To facilitate the CN cluster analysis, we represent a given atomic system as a graph $G = (V, E)$, where the atoms are the vertices, V, and the distance between two vertices, V_1 and V_2, is the weight for the edge, E, between those two atoms. The graph is stored in the form of an adjacency list. A set of common neighbors for atom i and atom j is given by:

$$CN_{ij} = \{k : d(i,k) \leq r_C \wedge d(j,k) \leq r_C\}$$

from which we can extract the clusters with different number of common neighbors. Figure 7 (right) shows a single 3-CN cluster in which two green spheres (Mg atoms) and one top red sphere (O atom) are three common neighbors for the remaining pair of the red spheres (O atoms).

Spheres of atomic movement

Various sets of displacement data are generated to characterize the extent and pattern of the atomic movement during simulation. In general, displacements are defined as

$$\Delta r_i = r_i^t - r_i^0, \quad \text{for } i = 1, 2, \ldots\ldots, N$$

Here, r_i^t and r_i^0 are the positions of ith atom in a given (at a particular time) and reference configuration, respectively. The data may represent differences of a given atomic configuration (r_i^t) from the initial ($r_i^{t=0}$) or previous ($r_i^{t-\Delta t}$) or next ($r_i^{t+\Delta t}$) configuration. The reference configuration can be the crystalline configuration (r_i^{crys}) as well. The other relevant differences are those involving the mean positions $c_i = \frac{1}{n_{steps}} \sum_{j=1}^{n_{steps}} p_i^j$ taken over the whole simulation period, where n_{steps} is the number of simulation steps, $p^j{}_i$ is position of ith atom at jth simulation step.

All these data represent discrete vector data, which are rendered using spheres and lines (Fig. 8). The magnitude of the vector is represented by the size of the sphere placed at each atomic site (p_i) in 3D space:

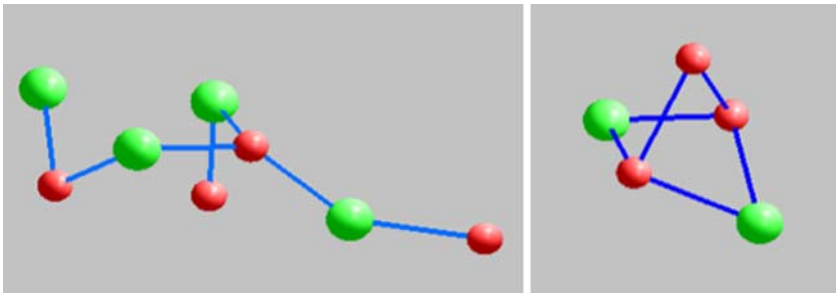

Fig. 7 Nearest-neighbor (*NN*) and common-neighbor (*CN*) clusters

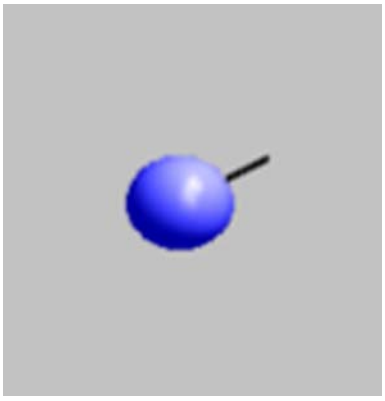

Fig. 8 Sphere-and-line representation of atomic displacement

$$r_i^s = f|\Delta r_i| + a,$$

where f is the scaling factor and a is the minimum radius given to each sphere. The direction is represented by a line segment, which points away from the surface of the sphere:

$$\text{line}\left(|\Delta r_i|p_i, |\Delta r_i|p_i + l\frac{\Delta r_i}{|\Delta r_i|}\right),$$

where Δr_i is the orientation vector, p_i is the center of the sphere, and l is the length of the line. In the case, where we are interested at the farthest positions the atoms reach during the whole simulation period from the mean positions, the centroid spheres are drawn at c_i's with the radii defined by $r_i = \max_{j=1:n_{\text{steps}}} \{d(c_i, p_i^j)\}$.

Visualization results for liquid data

In this section, we present a detailed visualization of the simulation data for liquid MgO and $MgSiO_3$ to understand the effects of pressure and temperature on their structural and dynamical behavior. In particular, we focus on atomic coordination, cluster structure and diffusion pattern.

Liquid MgO

We visualize the atomic coordination environment of liquid MgO using the data for 216-atom supercell at two conditions ($V1T1$) and ($V2T2$) using the coordination-encoded spheres (Fig. 9). Visualization implies that the coordination is not uniform throughout the system and relative contributions of different types (which range from threefold to ninefold) of coordination vary to some extent over the time. Out of 108 Mg atoms, there are 4 three- (black), 37 four- (red), 49 five- (yellow), 17 six- (green) and 1 seven- (cyan) fold coordinated Mg atoms at low compression (condition $V1T1$). At high compression (condition $V2T2$), there are 1 four- (red), 15 five- (yellow), 31 six- (green), 36 seven- (cyan), 19 eight- (blue) and 6 nine- (magenta) fold coordinated Mg atoms. Compression is shown to suppress the low C_{MgO} contributions (three-, four- and fivefold coordination) and enhance high C_{MgO} contributions (six-, seven- and eightfold coordination).

To understand cluster structure, we extract/visualize the common neighbor (CN) clusters as a function of the cutoff distance (r_C) (Fig. 10). In a 216-atom crystalline MgO supercell of dimension L, the minimum Mg–O distance is $L/6$, and the minimum O–O and Mg–Mg distances both are $(\sqrt{2}/6)L$. For $r_C \geq L/6$ and $< (\sqrt{2}/6)L$, there exist pairs only with two common neighbors. When $r_C \geq (\sqrt{2}/6)L$, higher-order clusters with 2, 3, 4, 6, and 8 common neighbors exist. In the liquid state, however, the largest number of common neighbors an atomic pair under consideration can have varies gradually from two to eight or higher value as the cutoff distance increases from 0.175 L to 0.25 L, as shown in Fig. 10. A similar trend is observed at condition $V2T2$ except that the largest number of the common neighbors is, on average, less by one than that at condition $V1T1$. Note that the position of the first minimum of the total RDF is 0.177 L at low compression so the relevant clusters contain mostly 2 and 3 common neighbors. On the other hand, r_{MIN} is 0.264 L at high compression so the relevant clusters contain as high as 9 common neighbors.

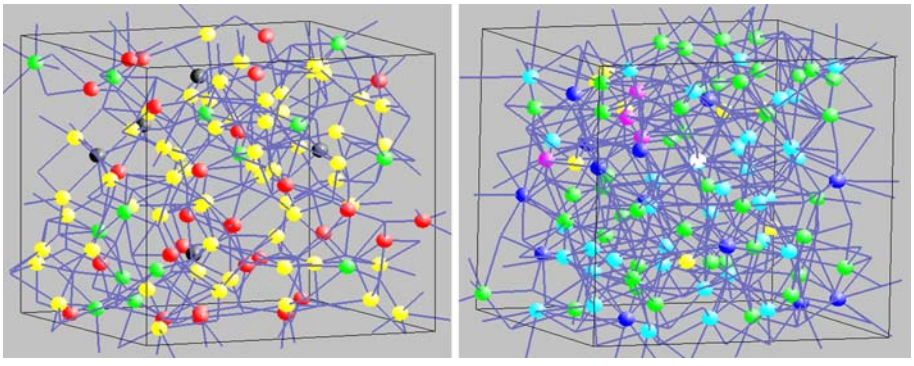

Fig. 9 Spatial distribution of Mg–O coordination number. *Left*, low compression (condition $V1T1$); *right*, high compression (condition $V2T2$)

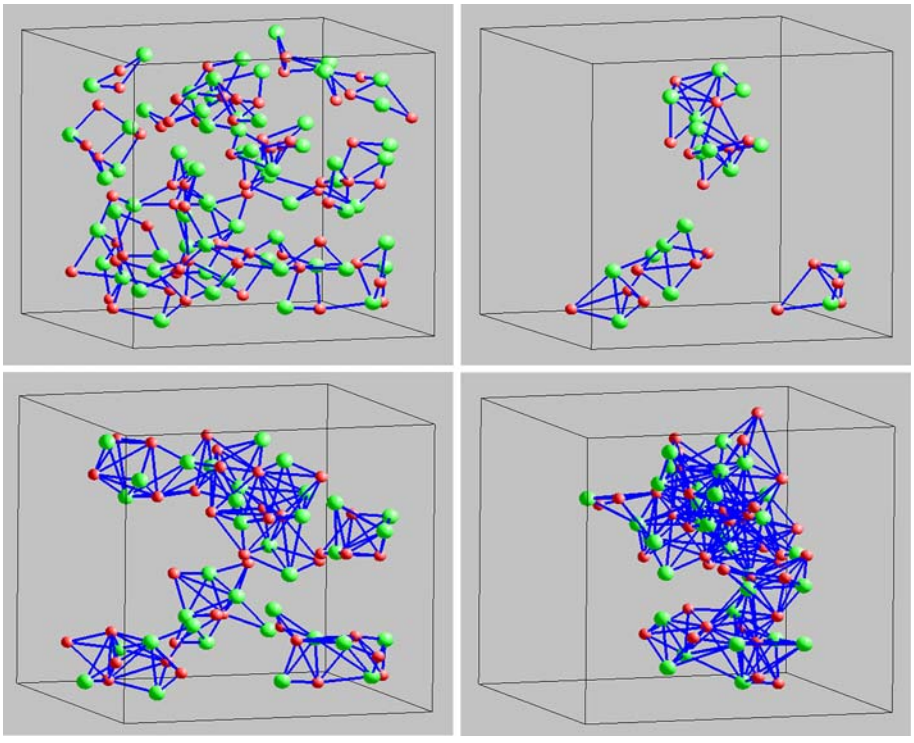

Fig. 10 Distance dependence of common neighbor clusters: 0.175 (*top left*), 0.200 (*top right*) 0.225 (*bottom left*) and 0.250 (*bottom right*) at condition *V*1*T*1

Liquid $MgSiO_3$

Spatial variation of Si–O and Mg–O coordination in the silicate liquid is visualized. At low compression (condition *T*1*V*1), the $MgSiO_3$ liquid shows mostly fourfold Si–O coordination, which is characteristic to the corresponding crystalline pyroxene phase. Visualization output reveals that there are 15 red (fourfold) and 1 yellow (fivefold) polygons (Fig. 11, left). Note that there is a total of 16 Si-polyhedra. However, the liquid structure lacks the elements of longer ranged order seen in the crystal and isolated polyhedra exist. With increasing compression, the number of fourfold coordination decreases whereas the number of five- and sixfold coordination increases. At medium compression (condition *V*2*T*2), the average value is about 5, compared to the value of 4.5 for majority—a high-pressure crystalline polymorph of the silicate. Three types of Si–O coordination (four-, five- and sixfold) exist in almost equal amount; the snapshot showing 6 red, 6 yellow and 4 green polyhedra (Fig. 11, center). Note that the contribution of fivefold coordination reaches its maximum at this compression. At high compression (condition *V*3*T*3), the Si–O coordination is mostly six-fold, which is characteristic of perovskite and post-perovskite phases (Horiuchi et al. 1987; Murakami et al. 2004; Oganov and Ono 2004). The liquid shows a few non-six-fold including both five- and sevenfold coordinated silicon atoms. Visualization snapshot shows 12 green (sixfold), 1 yellow (fivefold) and 3 cyan (sevenfold) polyhedra (Fig. 11, right). It also reveals that no polyhedron exists in isolation. However, there is no complete 3D framework of corner sharing octahedra as in the crystalline phase in which every octahedron shares its all corners with six other octahedra. Despite the absence of a complete corner-sharing, some polyhedra in the liquid

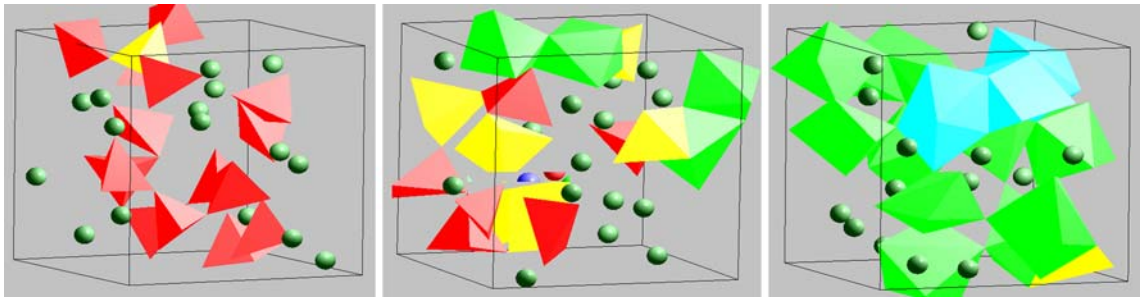

Fig. 11 Polyhedral representation of Si–O coordination environment in the silicate liquid at low (*V*1*T*1), medium (*V*2*T*2) and high (*V*3*T*3) compression from left to right

share edges and even faces with each other. In this sense, the liquid structure seems to be much more densely packed.

The cation coordination polyhedron such as SiO_n can be regarded as the fundamental unit in characterizing the atomic structure in response to temperature, pressure and composition. Figure 12 visualizes polyhedral distortion using the quadratic elongation parameter for the silicate liquid at three conditions (*V*1*T*1, *V*2*T*2 and *V*3*T*3). The individual polyhedra show different degrees of distortion as shown by their colors. At low and medium compression (*V*1*T*1 and *V*2*T*2), most polyhedra (black and red colored) show weak distortions whereas at high compression (*V*3*T*3), there are relatively few black and red colored polyhedra.

Mg–O coordination environment in silicate liquid also shows a similar trend (Fig. 13). At low compression, the coordination contains contributions from four-, five- and sixfold coordination. At medium compression, the contributions are from seven-, eight- and ninefold coordination, with the number of sevenfold coordinated Mg atoms being the maximum. Finally, at high compression, the number of cyan spheres (sevenfold) decreases whereas that of blue (eightfold) and magenta (ninefold) spheres increases. One can also see one or two white spheres (tenfold).

The NN clusters for the silicate liquid at condition *V*2*T*2 are extracted with three cutoff distances of r_{PEAK}, r_{AVG} and r_{MIN} obtained from the partial Si–O RDF function (Fig. 14). With r_{PEAK} and r_{AVG}, individual clusters are small consisting of only one Si atom and some O atoms. For the cutoff distance lying between r_{AVG}, and r_{MIN}, larger clusters consisting of more than one Si atoms are found. Finally, there is a single NN

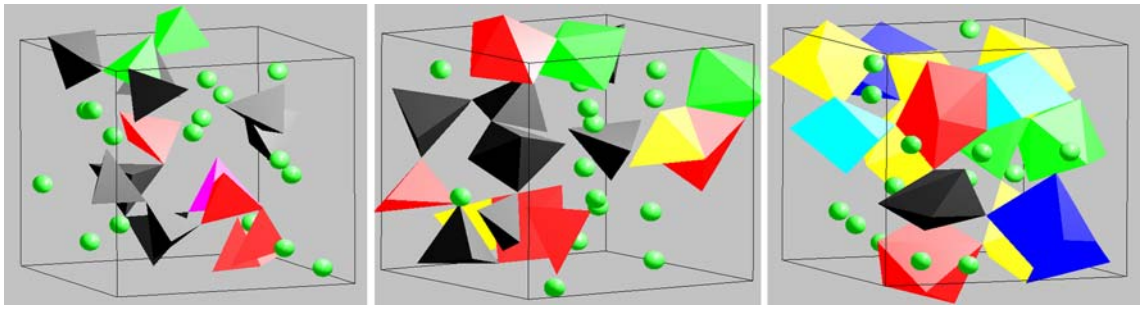

Fig. 12 Visualization of the quadratic elongation (λ_P) for liquid silicate at low (*V*1*T*1), medium (*V*2*T*2) and high (*V*3*T*3) compression from left to right. Note that *min* = 1.0 and *max* = 1.04 for λ_P

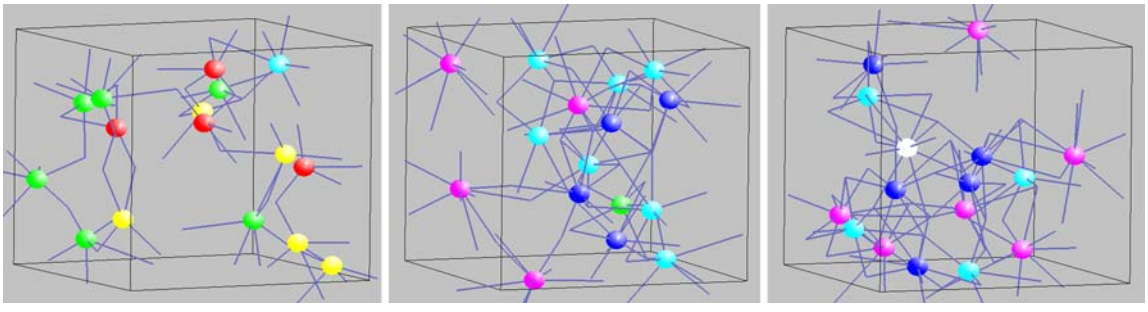

Fig. 13 Sphere representation of Mg–O coordination environment in the silicate liquid at low (*V*1*T*1), medium (*V*2*T*2) and high (*V*3*T*3) compression from left to right

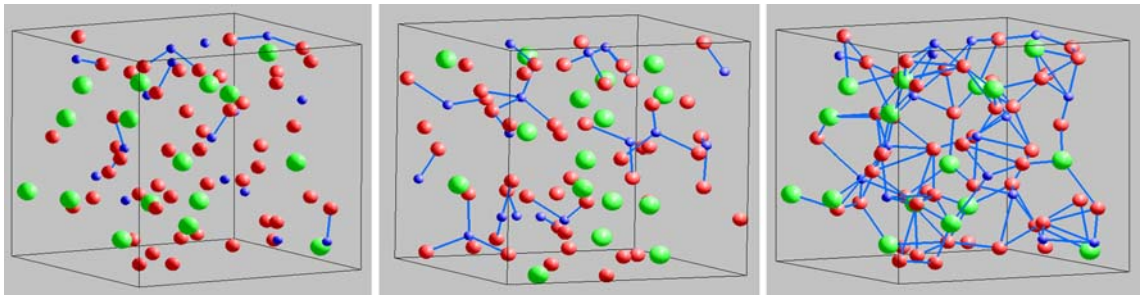

Fig. 14 Nearest-neighbor (*NN*) clusters in silicate liquid using r_{PEAK} (*left*), r_{AVG} (*center*) and r_{MIN} (*right*) at condition *V*2*T*2

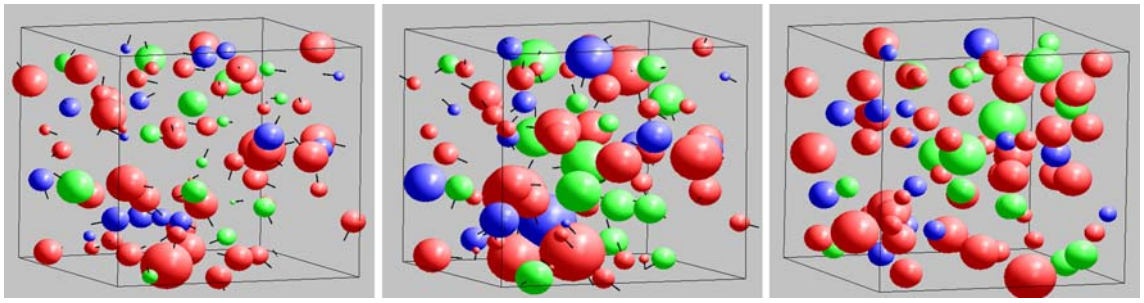

Fig. 15 Diffusion spheres for liquid silicate at medium compression (condition *V2T2*). *Left*: instantaneous displacement pattern (scaling factor = 20), *center*: displacement pattern over 500 time steps (scaling factor = 0.4), *right*: centroid spheres over 2000 time steps (scaling factor = 0.2)

cluster for r_{MIN}, which contains not only Si–O bonds but also contains some Mg–O, Mg–Si and O–O pairs.

Diffusion is an important dynamical phenomenon for a liquid phase. Simulations have shown that for both liquids temperature systematically enhances diffusion whereas pressure systematically suppresses it. Atomic diffusion pattern is explored by visualizing three types of displacement data (Fig. 15). They are instantaneous (positional differences between the present and previous steps), finite-time (positional differences between 2,500 and 3,000 steps) and maximum (differences between farthest and mean positions) displacement data. Visualization reveals that diffusion is not uniform throughout the system (i.e., among the constituent atoms of the same or different types). The spheres have different sizes and the lines showing the direction of atomic displacements are oriented along different directions. The red spheres (O atoms) are on average larger than the green (Mg atoms) and blue (Si atoms) spheres; and the blue spheres are the smallest ones. This means that the O atoms diffuse most among the three elements. Variation in the size of the centroid spheres is systematically much smaller than that of the instantaneous and finite-time spheres.

Conclusions

We have presented an efficient visualization scheme to interactively explore the atomistic simulation data for the detailed spatio-temporal information for the structure and dynamics of two geophysically relevant liquids, MgO and $MgSiO_3$. Our application-based visualization approach integrates several existing rendering and graph-theory techniques to fulfill the specific needs imposed by the sophisticated material modeling/simulation data. It deals with the original and on-the-fly-extracted data to understand the tendency of the atoms to form local structures and their stability over the time. In many cases, the physical relevance (atomic arrangement) needs to be rendered correctly, whereas, in other cases, only the information needs to be graphically rendered. Exploratory visual analysis of the liquid data has shown that the liquid structure is highly sensitive to compression: both Mg–O and Si–O coordination exhibit very complex environment with relative contributions of different types of coordination varying with compression. The cluster structure is shown to be strongly dependent on the cutoff distance used and to become increasingly more complex as compression increases. Finally, visualization reveals that the diffusion pattern in these liquids is highly non-uniform among the component atoms.

Acknowledgements This work is supported by the NSF Career (EAR 0347204) including EAR 0409074, ATM 0426601 and EAR-0409121.

References

Alfe D (2005) Melting curve of MgO from first principles simulations. Phys Rev Lett 94:Art. No. 235701

Allen MJ, Tildesley DJ (1987) Computer simulation of liquids. Oxford University Press, Oxford

Bhattarai D, Karki BB (2006) Visualization of atomistic simulation data for spatio-temporal information. In: WSCG'2006, the 14-th international conference in Central Europe on computer graphics, visualization and computer vision 2006. ISBN 80-86943-03-8

Blaisten-Barojas E (1984) Structural effects of three-body interactions on atomic microclusters. Kinam 6A:71

Chelikowsky JR, Derby JJ, Godlevsky VV, Jain M, Raty RY (2001) Ab initio simulations of liquid semiconductors. J Phys C 13:R817–R854

Hohenberg P, Kohn W (1964) Inhomogeneous electron gas. Phys Rev B 136:864–871

Honeycutt JD, Andersen HC (1987) Molecular dynamics study of melting and freezing of small Lennard-Jones clusters. J Phys Chem 91:4950–4963

Horiuchi H, Ito E, Weidner D (1987) Perovskite type $MgSiO_3$ single crystal X-ray diffraction study. Am Mineral 72:357–360

Humphrey W, Dalke A, Schulten K (1996) VMD: visual molecular dynamics. J Mol Graph 14:33–38

Jarvis RA, Patrick EA (1973) Clustering using a similarity measure based on shared near neighbors. IEEE Trans Comp C-22:615–624

Karki BB, Bhattarai D, Stixrude L (2006) First-principles calculations of structural, dynamical and electronic properties of liquid MgO. Phys Rev B (in press)

Kohn W, Sham L (1965) Self-consistent equations including exchange and correlation effects. Phys Rev A 140:1133–1138

Kokaji A (1999) XcrysDen-a new program for displaying crystalline structures and electron densities. J Mol Model 17:176–179

Kokaji A (2003) Computer graphics and graphical user interfaces as tools in simulations of matter at the atomic scale. Comput Mater Sci 2:155–168

Kraulis PJ (1991) Molscript—a program to produce both detailed and schematic picts of protein structures. J Appl Crystallogr 24:946–950

Kresse G, Furthmuller J (1996) Efficiency of ab-initio total energy calculations for metals and semiconductors using a plane-wave basis set. Comput Mater Sci 6:15–50

Li J (2005) Atomistic visualization. In: Yip S (ed) Handbook materials modeling. Springer, Berlin Heidelberg New York, pp 1051–1068

Murakami M, Hirose K, Kawamura K, Sata N, Ohishi Y (2004) Post-perovskite phase transition in $MgSiO_3$. Science 304:855–858

Oganov AR, Ono S (2004) Theoretical and experimental evidence for a post-perovskite phase of $MgSiO_3$ in Earth's D layer. Nature 430:445–448

Robinson K, Gibbs GV, Ribbe PH (1971) Quadratic elongation—quantitative measure of distribution in coordination polyhedra. Science 172:567–570

Sharma A, Haas A, Nakano A, Kalia RK, Vashistha P, Kodiyalam S, Miller P, Zhao W, Liu X, Campbell TJ (2003) Immersive and interactive exploration of billion-atom systems. Presence 12:85–95

Shreiner D, Woo M, Neider J (2004) OpenGL programming guide, 4th edn. Addison-Wesley, New York

Stixrude L, Karki BB (2005) Structure and freezing of $MgSiO_3$ liquid in Earth's mantle. Science 310:297–299

Thomas NW (1989) Crystal structure–physical property relationships in perovskites. Acta Crystallogr B 45:337–344

Trave A, Tangney P, Scandolo S, Pasquarello A, Car R (2002) Pressure-induced structural changes in liquid SiO_2 from ab initio simulations. Phys Rev Lett 89:Art No. 245504